Loss mechanisms of surface plasmon polaritons on gold probed by cathodoluminescence imaging spectroscopy.

M. Kuttge,[1,a] E. J. R. Vesseur,[1] J. Verhoeven,[1] H. J. Lezec,[2,b] H. A. Atwater,[2] and A. Polman[1]

[1]*Center for Nanophotonics, FOM-Institute AMOLF, Kruislaan 407, 1098 SJ, Amsterdam, Netherlands*
[2]*Thomas J. Watson Laboratories of Applied Physics, California Institute of Technology, Pasadena, California 91125, USA*

We use cathodoluminescence imaging spectroscopy to excite surface plasmon polaritons and measure their decay length on single crystal and polycrystalline gold surfaces. The surface plasmon polaritons are excited on the gold surface by a nanoscale focused electron beam and are coupled into free space radiation by gratings fabricated into the surface. By scanning the electron beam on a line perpendicular to the gratings, the propagation length is determined. Data for single-crystal gold are in agreement with calculations based on dielectric constants. For polycrystalline films, grain boundary scattering is identified as additional loss mechanism, with a scattering coefficient $S_G = 0.2\%$. © *2008 American Institute of Physics.* [DOI: 10.1063/1.2987458]

Surface plasmon polaritons (SPPs) are electromagnetic waves bound to the interface between a metal and a dielectric.[1] They are being intensively investigated due to their possible application in nanophotonic integrated circuits, sensors, solar cells, and other devices that take advantage of the strong optical field confinement at the metal/dielectric interface. SPPs decay by Ohmic losses in the metal, which are largest for wavelengths close to the surface plasmon resonance. In addition, scattering from surface roughness, grain boundaries, and other imperfections causes losses. Ohmic losses can be readily calculated from optical constants that can be measured independently. In practice, experimental loss rates are often much higher than the calculated Ohmic loss.[2] Calculation of scattering processes is difficult because they depend on minute details in the structure. Therefore, experimental techniques are required to identify the loss processes for SPPs. If these mechanisms are known, metal fabrication techniques can be optimized so that metal structures with longer SPP propagation lengths can be made.

In this letter, we use cathodoluminescence (CL) imaging spectroscopy to measure the SPP decay[3–5] and present a detailed study of the propagation length of SPPs on gold surfaces. We compare a single-crystalline gold surface with polycrystalline gold films with different grain sizes. We measure the SPP decay close to the plasmon resonance with nanometer resolution and extract the decay constants for a broad range of wavelengths. We show that losses are determined both by Ohmic losses and scattering at grain boundaries, and that surface scattering plays only a minor role.

In CL an electron beam impinges onto the gold surface to create a perturbation in the density of conduction electrons. The corresponding effective dipole oscillation is the source for CL. The dipole decays by emitting into the far field (transition radiation[6]) and by exciting SPPs.[7,8] In our experiment, the excited SPPs propagate over the surface and are coupled to the far field using a grating structured into the metal surface. By measuring the amount of light coupled out from the grating as a function of distance between excitation point and grating, the SPPs propagation length can be determined.

We prepared three different samples for our measurements. One sample consists of a single-crystalline gold pellet with a thickness of 1 mm. The surface was polished via chemical polishing to subnanometer roughness as confirmed by atomic force microscopy (AFM). Two more samples were produced by electron-beam evaporation of a 120 nm thick gold film on a silicon substrate. Before the evaporation, the silicon substrates were cleaned in vacuum with a 300 eV argon ion beam. The films were evaporated at a rate of 0.05 nm/s under a pressure of 3×10^{-7} mbar. To achieve different grain sizes for the films, one sample substrate was cooled during evaporation to liquid nitrogen temperature, while the other was kept at room temperature. To reduce surface roughness of the evaporated metal, both samples were irradiated with 300 eV argon ions at the last 30 s of the evaporation.[9] The two-dimensional surface profiles of the evaporated films measured with AFM are shown in Figs. 1(a) and 1(b). Grain boundaries were easily identified in AFM, and the average grain diameter was determined to be $d = 80$ nm for the film deposited at room temperature (a) and $d = 20$ nm for the film deposited onto a cooled substrate (b). The root-mean-square surface roughness was 1.6 and 1.3 nm for the room temperature and cooled deposition, respectively. Grating structures were milled into the surfaces of the metal with a 30 keV focused ion beam from a liquid gallium source. The gratings consisted of ten grooves with a period of 400 nm and a groove depth of 50 nm [Fig. 1(c)]. The single-crystalline gold sample will be referred as *x*-Au, the polycrystalline sample as poly-LN and poly-RT for the cooled and the room temperature evaporated film, respectively.

We used the 30 kV electron beam of FEI XL-30 scanning electron microscope using a field-emission source focused to a beam diameter of approximately 5 nm to excite SPPs on the gold surfaces. The scanning electron beam

―――――――――
[a]Electronic mail: kuttge@amolf.nl.
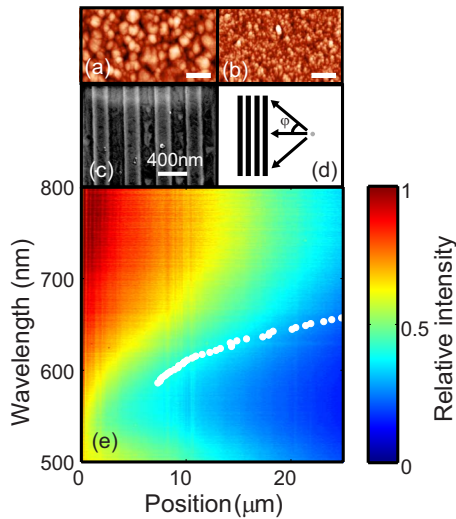[b]Present address: Center for Nanoscale Science and Technology, NIST, Gaithersburg, MD, USA.

FIG. 1. (Color online) [(a) and (b)] AFM images of gold films evaporated at room temperature (a) and onto a cooled substrate (b). The scale bar is 100 nm and the height variation is 1 nm. (c) Scanning electron micrograph image of a grating fabricated in the single-crystal gold substrate. (d) Schematic drawing of SPPs propagating from the source to the grating over broad angular range. (e) CL intensity as a function of detection wavelength and distance to a grating in a single-crystalline gold surface. The edge of the grating at zero distance and the CL intensity was normalized to the intensity at zero distance for each wavelength. The white dot shows the fitted SPP propagation length L_{SPP} for this sample.
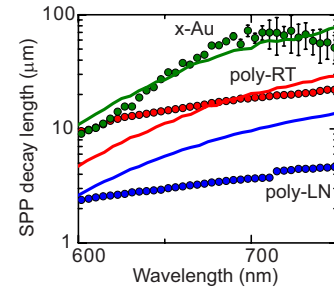

FIG. 2. (Color online) SPP propagation length as a function of wavelengths for three different samples from fits to measurements as in Fig. 1(e). The blue dots are for single-crystalline gold (*x*-Au) and the red and green dots are for polycrystalline gold films deposited at room temperature (poly-RT) and liquid-nitrogen temperature (poly-LN), respectively. The solid lines are propagation lengths calculated from the dielectric constants measured for the respective samples.

passes through a 1-mm-diameter hole in a parabolic mirror that is positioned above the sample. The light coming from the sample was collected using the parabolic mirror with an acceptance angle of about 1.4π sr. The collected light was sent through a monochromator and spectrally resolved with a charge coupled device array detector with a resolution of approximately 10 nm.

We measured the CL intensity as a function of position on a line normal to the grating up to a distance of 25 μm from the grating. The electron beam was scanned with a step size of 100 nm and at each position a spectrum was measured with an integration time of 10 s. The measured emission spectrum ranges from around 500 nm to the near infrared region and peaks around 600 nm. The measured spectrum due to SPPs for a fixed position is determined by the excitation spectrum of SPPs by the electron beam, the propagation losses, and the wavelength dependent outcoupling efficiency of the grating and the spectral response of the CL system. Since we are interested in the relative decay of the CL intensity, for each wavelength the measured CL signal was normalized to the intensity measured at the edge of the grating.

Figure 1(e) shows the normalized CL intensity for a line scan close to the grating as a function of position and detection wavelength for the single-crystalline gold sample. The edge of the grating is located on the left side at zero distance. As can be seen, for every wavelength the CL intensity decreases for increasing distance. For wavelengths above 550 nm, the decrease in CL intensity is weaker for longer wavelengths, corresponding to a larger propagation for longer wavelengths. For 550 nm a minimum of the propagation length is observed; for shorter wavelengths the propagation length appears increased, as will be discussed.

The CL intensity $I(x)$ for the electron beam at a distance x away from the grating is given by the initial SPP generation rate $I_0(\lambda, \phi)$, the SPP decay length $L_{SPP}(\lambda)$, and the grating outcoupling efficiency $\alpha(\lambda, \phi)$, which depends on the incident angle ϕ relative to the grating normal [see schematic in Fig. 1(d)]:

$$I(x) = I_{TR} + \frac{1}{2\pi} \int_{-\pi/2}^{\pi/2} \alpha(\lambda, \phi) I_0(\lambda, \phi) \exp\left[\frac{-x}{L_{SPP}(\lambda)\cos(\phi)}\right] d\phi. \tag{1}$$

Equation (1) also includes a constant background I_{TR} to account for the transition radiation. To obtain the plasmon propagation length $L_{SPP}(\lambda)$, we fitted Eq. (1) for each wavelength in the data set of Fig. 1(e) assuming an angle-independent coupling efficiency $a(\lambda, \phi) = 1$. The results of the fits for L_{SPP} are shown in Fig. 1(e) as white dots. We have plotted the values for L_{SPP} only above 600 nm. In this region, we observe an increase in propagation length with wavelength as expected.

Interestingly, as can be seen in Fig. 1(e) for wavelengths shorter than 600 nm, we observe CL intensity farther away from the grating. This would mean that the SPP propagation length seems to increase with the decreasing wavelength. In this wavelength range SPPs are not purely bound to the surface, as their real part of the normal wavevector component k_z increases strongly with the decreasing wavelength. The resulting radiative loss causes a strong decrease in propagation of bound SPPs. However, in the present experiment, the effect of this loss process, radiation, is collected by the detection system. As Eq. (1) does not account for this effect, these data are not further analyzed here.

A similar analysis as in Fig. 1(e) for the single-crystalline sample was done for the two polycrystalline samples. Figure 2 (symbols) shows the fitted propagation lengths for the three different samples. The spread in data extracted from different measurements for the same sample was approximately 10%–20%. For fitted propagation lengths that are longer than the scan range of 50 μm, we have added error bars. The longest propagation lengths are found for the single-crystalline gold sample. The shortest propagation lengths are found for the polycrystalline samples with the smallest grain size.

Considering only Ohmic losses, the SPP propagation length can be calculated from the imaginary part of the SPP wave vector k_x,

$$L_\Omega = \frac{1}{2 \, \mathrm{Im} \, k_x}. \qquad (2)$$

For a semi-infinite metal in air, the wavevector is given by $k_x = \lambda/(2\pi)\sqrt{\epsilon/(\epsilon+1)}$ with ϵ the dielectric constant of gold and λ the free-space wavelength. For a thin film on a substrate leakage radiation must also be taken into account. We have calculated the dispersion relation for the three-layer system of a gold film in air on a silicon substrate and derived L_Ω from k_x, as in Eq. (2) for the polycrystalline films.[1] The dielectric constants of the three different samples were measured using ellipsometry.

The drawn lines in Fig. 2 show the propagation lengths for SPPs on our three samples calculated from these dielectric constants. Note that these include no free parameters. Already the calculated propagation lengths differ for the studied samples by an order of magnitude, mainly due to different dielectric constants. The large variation in dielectric constants can be explained by a reduction in the mean free path for electrons by introduction of grain boundaries, voids, and roughness.[10] For single-crystalline gold, for wavelengths longer than 600 nm the measured values of propagation length are in good agreement with the calculations. For the large-grain polycrystalline (poly-RT) sample data and calculation are in reasonable agreement for longer wavelengths. For the small grain size sample, the experimental data lie well below the calculation for larger wavelengths. This indicates that additional loss mechanisms are involved, which decrease the SPP propagation length and cannot be described by Ohmic losses.

One possible additional loss mechanism is scattering at surface roughness of the metal. However, given the small surface roughness of our samples as measured using AFM, this effect is negligible.[11] With the given geometrical parameters of our samples, the contribution of scattering at roughness can be estimated to be a factor of 500 smaller than the Ohmic losses. Even more, as the roughness values for all our samples are very similar, the effect of scattering at roughness should be similar for all samples. Therefore, we cannot explain the deviations in SPPs propagation length by surface roughness.

Next, we consider grain boundary scattering of SPPs. In few other studies, the effect of grain boundary scattering has been considered as a loss mechanism for both the bulk and surface plasmons.[12–14] The proposed reason for the scattering lies mainly in inhomogeneities of the free-electron gas due to grain boundaries. As far as we know, no quantitative studies on the effect of grain boundary scattering of SPPs have been published. In a simple model for the grain boundary scattering, the effective propagation length equals $L_G = S_G/d$, with S_G the grain boundary scattering coefficient and d the average grain diameter (for $d \ll L_G$). Adding this loss term to the Ohmic losses, we fitted our data for $\lambda \geqslant 600$ nm for the two polycrystalline samples, with d taken from AFM measurements and S_G as a free parameter, but identical for both samples. We find a reasonable fit of the calculation with both data sets assuming $S_G = 0.2\%$. The results of our calculations are plotted as lines in Fig. 3 together with the measured curves for the polycrystalline films. So far, a model
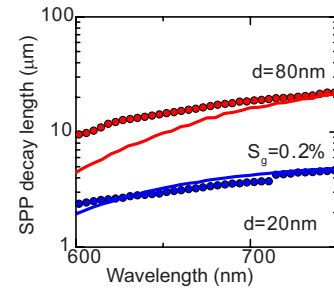

FIG. 3. (Color online) SPP propagation length as a function of wavelengths for two different grain sizes. The symbols are the decay lengths as obtained from measurements. The drawn curves are calculated including grain boundary scattering for grain sizes of 20 and 80 nm, respectively, and a grain boundary scattering coefficient $S_G = 0.2\%$.

for Ohmic and scattering losses is found that fits well the data for all three samples in the wavelength range above 600 nm.

In conclusion, we have performed CL imaging spectroscopy to measure the propagation length of SPP propagation on single-crystalline and polycrystalline gold surfaces. From the measurements, we have determined the SPP decay lengths as a function of wavelength in the 600–750 nm range. Largest propagation lengths ($10-80$ μm), in agreement with optical constants, are found for single-crystalline Au. Much reduced propagation lengths are found for polycrystalline films. We find that grain boundary scattering is an important plasmon loss mechanism in polycrystalline thin films. The data is consistently fitted using a grain boundary scattering coefficient of 0.2%.

[1] H. Raether, *Surface Plasmons on Smooth and Rough Surfaces and on Gratings* (Springer, Berlin, 1988).
[2] E. M. Schmidlin and H. J. Simon, Appl. Opt. **28**, 3323 (1989).
[3] J. T. van Wijngaarden, E. Verhagen, A. Polman, C. E. Ross, H. J. Lezec, and H. A. Atwater, Appl. Phys. Lett. **88**, 221111 (2006).
[4] M. V. Bashevoy, F. Jonsson, A. V. Krasavin, N. I. Zheludev, Y. Chen, and M. I. Stockman, Nano Lett. **6**, 1113 (2006).
[5] M. V. Bashevoy, F. Jonsson, K. F. MacDonald, Y. Chen, and N. I. Zheludev, Opt. Express **15**, 11313 (2007).
[6] N. Yamamoto, H. Sugiyama, and A. Toda, Proc. R. Soc. London, Ser. A **452**, 2279 (1996).
[7] G. W. Ford and W. H. Weber, Phys. Rep. **113**, 195 (1984).
[8] F. J. García de Abajo, Rev. Mod. Phys. **79**, 1267 (2007).
[9] E. J. Puik, M. J. van der Wiel, H. Zeijlemaker, and J. Verhoeven, Rev. Sci. Instrum. **63**, 1415 (1992).
[10] D. E. Aspnes, E. Kinsbron, and D. D. Bacon, Phys. Rev. B **21**, 3290 (1980).
[11] D. L. Mills, Phys. Rev. B **12**, 4036 (1975).
[12] P. Dawson, K. B. Alexander, J. R. Thompson, J. W. Haas, and T. L. Ferell, Phys. Rev. B **44**, 6372 (1991).
[13] V. Krishan and R. H. Ritchie, Phys. Rev. Lett. **24**, 1117 (1970).
[14] J. R. Sambles, Solid State Commun. **49**, 343 (1984).